Available online at www.sciencedirect.com

ScienceDirect

International Journal of Solids and Structures 45 (2008) 850–867

INTERNATIONAL JOURNAL OF SOLIDS AND STRUCTURES

www.elsevier.com/locate/ijsolstr

Comparison between the relaxation spectra obtained from homogenization models and finite elements simulation for the same composite

Romina B. Barello, Martin Lévesque *

CREPEC, Département de Génie Mécanique, École Polytechnique de Montréal, C.P. 6079, Succ. Centre-ville, Montréal, Canada H3C 3A7

Received 23 April 2007; received in revised form 3 July 2007
Available online 14 September 2007

Abstract

The objective of this work is to determine the relaxation spectrum of spherical particles reinforced viscoelastic and isotropic composites from 3D Finite Elements (FE) simulations of the microstructure. The matrix and the reinforcements are assumed to be incompressible and Maxwellian. The spectra obtained from the FE simulations are compared with those obtained from analytical homogenization models. This paper presents the procedure used for generating the FE models as well as the procedure used for obtaining relaxation spectra meeting the thermodynamics requirements imposed on linear viscoelastic materials. It seems that the relaxation spectrum for the microstructure studied in this paper is composed of a negligible continuous part and a discrete part of higher intensity. In any case, the resulting material does not have a Maxwellian behavior.

Keywords: Stress relaxation; Finite Element Analysis (FEA); Homogenization; Unit cell

1. Introduction

Homogenization techniques can be used for predicting the effective behavior of composites based on information related to the microstructure. There are two principal categories of homogenization methods: the analytical methods and the numerical methods. Researchers like Gusev (1997), Segurado and LLorca (2002) and Mishnaevsky (2004) have worked on the effective elastic properties prediction by performing Finite Element (FE) analyses of three-dimensional material microstructure unit cells. Brinson and Knauss (1992) and Nguyen Viet et al. (1995) have performed 2D FE analyses of linear viscoelastic composites. Huet (1990) and Hazanov and Huet (1994) proposed bounding relations for the effective properties using uniform and mixed boundary conditions, respectively. They found that if smaller material specimens are selected and uniform boundary conditions are applied, a bias is introduced on the effective properties calculation. Kanit et al. (2003) have pro-

* Corresponding author.
E-mail address: martin.levesque@polymtl.ca (M. Lévesque).

0020-7683/$ - see front matter
doi:10.1016/j.ijsolstr.2007.09.002

posed a statistical procedure for determining the Representative Volume Element (RVE) size. They verified that using periodic boundary conditions leads to smaller RVE size than using displacement or traction uniform boundary conditions. Xia et al. (2006) have demonstrated that in displacement-based finite element method, the application of periodical boundary conditions on the displacements guarantees the periodicity of the tractions.

The first analytical homogenization models were developed for linear elastic materials. These results were extended to non linear materials as well as to linear viscoelastic materials. The homogenization of linear viscoelastic materials is classically performed using the viscoelastic correspondence principle and the Laplace–Carson Transforms (LCT). The procedure consists in applying the LCT to the linear viscoelastic constitutive theories and insert these symbolic mechanical properties into a linear elastic homogenization model. The overall properties are obtained by the LCT inversion. Hashin (1965) has used such principle for unidirectional fiber composites; Wang and Weng (1992) and Lévesque et al. (2004) with the Mori-Tanaka (MT) scheme and Laws and McLaughlin (1978), Beurthey and Zaoui (2000) and Brenner et al. (2002) with the Self-Consistent (SC) scheme, amongst others.

This work focuses on linear viscoelastic composite materials. The objective of this work is to compare the relaxation spectrum of composite materials constituted of incompressible, isotropic, viscoelastic and Maxwellian phases obtained by numerical homogenization and analytical models. The microstructure studied consists in spherical reinforcements randomly distributed into a matrix. FE meshes of RVE of such microstructure are built and their solutions are considered as the "exact solution". The analytical homogenization models tested are MT, SC and Torquato (TOA) (Torquato, 1998). The FE models as well as the simulations are described at Section 2. The numerical method used for obtaining the relaxation spectra from the FE simulations is described at Section 3. Comparisons between the FE and the analytical approaches results are presented at Section 4.

2. Finite element model

2.1. Obtaining the finite element models

The composite is modeled as a cube containing spherical reinforcements. The Random Sequential Adsorption algorithm (Segurado and LLorca, 2002) has been used for obtaining a spatially random sphere distribution. Conditions of minimum distance between each sphere and between each sphere and each cube face (Segurado and LLorca, 2002) have been imposed. The coordinates of the centre of the first sphere are randomly generated. If the distances between the sphere and each cube face are greater than an established value, the sphere is accepted. Otherwise, the sphere is rejected and the coordinates of a new sphere are generated again until the distance condition mentioned above is met. The following spheres are generated sequentially. The centre coordinates of a new sphere are randomly generated and the distances between the sphere and the cube faces are verified. Then, the distances between the new sphere and those previously created must be inferior to a certain value. In this study, the spheres were randomly distributed into a cube of $10 \times 10 \times 10$ mm. The spheres radii were calculated for obtaining the desired reinforcement volume fraction. The distances between the centers of two spheres had to be greater than $2.07r$ mm and the distances from the cube faces greater than $0.1r$ mm (r stands for the sphere radius). Periodic boundary conditions were applied to the cube's surfaces since it leads to a smaller RVE than with homogeneous tractions or displacements (Kanit et al., 2003). Periodic RVE were created for facilitating the application of this type of boundary conditions.

The mesh of the unit cell was created with the commercial software `ANSYS 10.0`. Fig. 1 shows the solid model of a unit cell containing 50 spheres for a volume fraction ζ of 25%. Constraint equations were imposed between nodes lying on opposite faces for applying the periodic boundary conditions. The three cube faces intersecting the Cartesian coordinate system origin were meshed in a first time with surface elements (6-noded triangles). Then, these meshes were copied to the opposite faces. Finally, the volumes were meshed with 10-noded tetrahedra. Fig. 2 shows the mesh corresponding to the reinforcement. This mesh was then exported to `ABAQUS/Standard 6.5` for the calculations.

Periodic displacements fields can be expressed as (Michel et al., 1999):

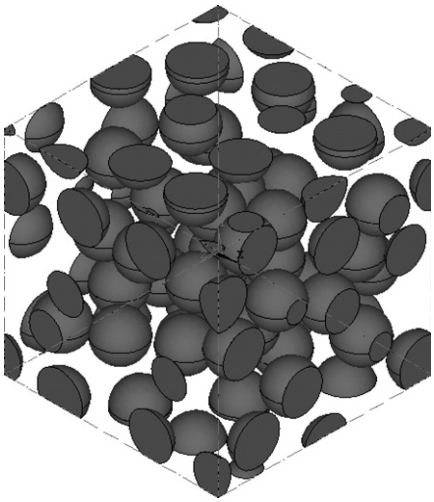

Fig. 1. Solid model. Cube containing 50 spheres. Volume fraction $\zeta = 25\%$.

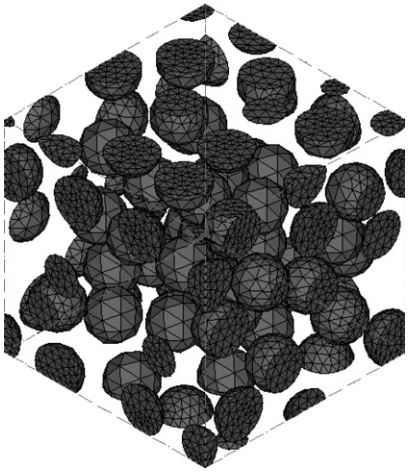

Fig. 2. Mesh of the reinforcements shown at Fig. 1.

$$\boldsymbol{u}(\boldsymbol{x}) = \mathbf{E} \cdot \boldsymbol{x} + \boldsymbol{u}^{*}(\boldsymbol{x}) \tag{2.1}$$

where $\boldsymbol{u}(\boldsymbol{x})$ is the displacement vector corresponding to the position vector $\boldsymbol{x}$, $\mathbf{E}$ is the overall strain in the elementary cube and $\boldsymbol{u}^{*}(\boldsymbol{x})$ is a periodic fluctuation. The spatial average of $\boldsymbol{u}^{*}(\boldsymbol{x})$ is equal to zero. This periodic field takes the same values in a pair of points that are on opposite faces (i.e. sharing two of their coordinates).

The fluctuation $\boldsymbol{u}^{*}(\boldsymbol{x})$ can be eliminated with the following set of equations:

$$\begin{aligned}
&\boldsymbol{u}(0, x_2, x_3) + \mathbf{E} \cdot (L, 0, 0) = \boldsymbol{u}(L, x_2, x_3) \\
&\boldsymbol{u}(x_1, 0, x_3) + \mathbf{E} \cdot (0, L, 0) = \boldsymbol{u}(x_1, L, x_3) \\
&\boldsymbol{u}(x_1, x_2, 0) + \mathbf{E} \cdot (0, 0, L) = \boldsymbol{u}(x_1, x_2, L)
\end{aligned} \tag{2.2}$$

where L is the cube length. When setting $\boldsymbol{u}(\mathbf{0}) = \mathbf{0}$ to prevent rigid body motions, the components of $\mathbf{E}$ as a function of the displacements of some nodes can be obtained and relations between the displacements of these nodes are established due to the symmetry of $\mathbf{E}$, namely:

$$\begin{aligned}
&\frac{u_1(L,0,0)}{L} = E_{11}, \quad \frac{u_2(L,0,0)}{L} = E_{12}, \quad \frac{u_3(L,0,0)}{L} = E_{13} \\
&\frac{u_1(0,L,0)}{L} = E_{21}, \quad \frac{u_2(0,L,0)}{L} = E_{22}, \quad \frac{u_3(0,L,0)}{L} = E_{23} \\
&\frac{u_1(0,0,L)}{L} = E_{31}, \quad \frac{u_2(0,0,L)}{L} = E_{32}, \quad \frac{u_3(0,0,L)}{L} = E_{33}
\end{aligned} \tag{2.3}$$

2.2. Simulation description

Relaxation tests were simulated. In a relaxation test, the strains are suddenly applied from 0 to a certain value, $\boldsymbol{\varepsilon}_t$ at $t = 0$. This strain is kept constant and the stresses are measured. In this study, we applied an overall shear deformation E_{12} and computed the overall stress Σ_{12}. The sudden strain jump was in fact applied over 5×10^{-5} s and the final simulation time was 5 s. It was observed that applying the strain jump over 1×10^{-7} s produced a difference of less than 0.02% in Σ_{12} right after the assumed strain jump. Therefore, it was assumed that $\Sigma_{12}(t = 5 \times 10^{-5}) \cong \Sigma_{12}(t = 0)$. The composite phases were modeled as linear viscoelastic, isotropic, incompressible and Maxwellian. It should be noted that these values were arbitrarily chosen and do not represent any real material. The objective here is to study the sensitivity of the homogenization models to the contrasts between each phase. The shear relaxation modulus of each phase was defined as:

$$\mu_i(t) = \mu_i^0 \exp\left[-\frac{t}{\tau_i}\right] \tag{2.4}$$

where μ_i^0 corresponds to the instantaneous modulus of the phase i and τ_i corresponds to the relaxation time of the phase i. Table 1 lists the material properties used in the FE simulations for two levels of contrast (η) between phase properties. Both the instantaneous shear modulus and the relaxation time were varied simultaneously.

The effective response of the composite was obtained by calculating the volume average of the stresses and strains. The FE code computes the local stresses and strains at each integration point. In addition, a volume is associated to each integration point. The subroutine `URDFIL` built in `ABAQUS/Standard 6.5` has been used for computing these volume averages from the integration points results.

The RVE size has been studied by varying the number of spheres within the FE model. The evolution of the stress–strain curves was studied as a function of the RVE size. FE models with 5, 10, 15, 20, 25, 30, 40 and 50 spheres were tested depending on the volume fraction and contrast between phases. For each RVE size, at least 6 simulations were performed. If the mean effective shear relaxation modulus of the composite did not vary significantly when the RVE size was increased, the RVE size was considered to have been attained. Figs. 3–6 show the mean shear relaxation modulus for the first computation time of each RVE size studied, for the case $\eta = 10$, for 10%, 15%, 20% and 25% volume fractions, respectively. The error bars on the figures represent a 95% confidence interval on the mean value (it is assumed that the mean effective response obeys a normal distribution). This applies to all the error bars in this paper. For the case $\eta = 100$, only two volume fractions were studied: 10% and 20%. Figs. 7 and 8 show the shear relaxation modulus for the first computation time of each RVE size studied for 10% and 20% volume fractions, respectively. For all the cases studied, a statistically significant difference (in the sense of a 95% confidence interval) on the mean relaxation shear modulus has been observed between the smallest and the largest RVEs plotted in Figs. 3–6. However, for most cases, no statistically significant difference has been observed between the mean shear relaxation modulus

Table 1
Material properties used for the FE simulations for $\eta = 10$ and $\eta = 100$

Phase	$\eta = 10$		$\eta = 100$	
	μ^0 (Pa)	τ_i (s)	μ^0 (Pa)	τ_i (s)
Matrix	8.67×10^7	5×10^{-1}	8.67×10^6	5×10^{-1}
Reinforcement	8.67×10^8	5×10^{-2}	8.67×10^8	5×10^{-3}

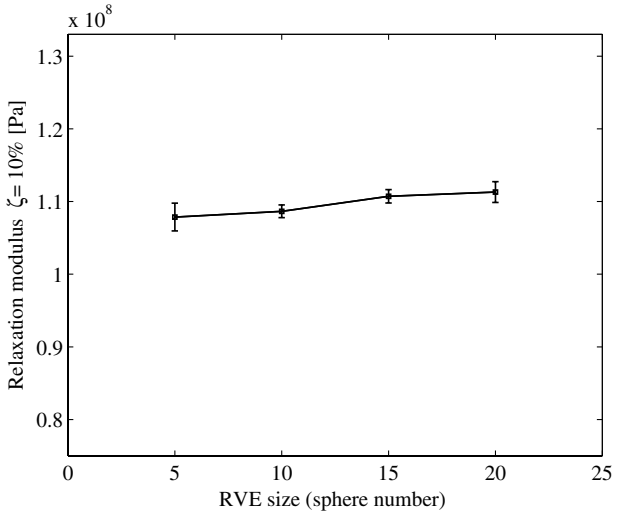

Fig. 3. Mean shear relaxation modulus for each RVE size (5, 10, 15 and 20 spheres) at $t = 0$. $\zeta = 10\%$. The error bars are a 95% confidence interval on the mean value. $\eta = 10$.

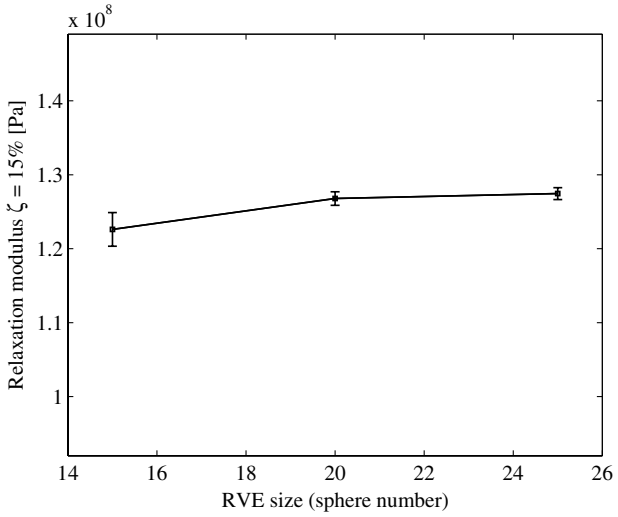

Fig. 4. Mean shear relaxation modulus for each RVE size (15, 20 and 25 spheres) at $t = 0$. $\zeta = 15\%$. The error bars are a 95% confidence interval on the mean value. $\eta = 10$.

for the intermediate RVE sizes studied. Considering the relatively narrow confidence intervals, it would seem that the biases in the mechanical properties have been cleared and that the RVEs have been reached. The simulations used for obtaining the relaxation spectra were those obtained for the largest RVE size. It should be noted that it was not possible to obtain larger RVEs than 50 spheres due to mesh limitations. So, for $\eta = 10$, for $\zeta = 10\%$ and RVE $= 20$, the instantaneous relaxation modulus was $11.1 \times 10^7 \pm 1.2\%$, for $\zeta = 15\%$ and RVE $= 25$, it was $12.76 \times 10^7 \pm 0.63\%$, for $\zeta = 20\%$ and RVE $= 30$, it was $14.51 \times 10^7 \pm$ 1.7% and for $\zeta = 25\%$ and RVE $= 50$, it was $16.86 \times 10^7 \pm 1.35\%$; for $\eta = 100$, for $\zeta = 10\%$ and RVE $= 20$, it was $1.28 \times 10^7 \pm 2.9\%$ and for $\zeta = 20\%$ and RVE $= 50$, it was $2.075 \times 10^7 \pm 2.6\%$.

The isotropy was verified by applying E_{12}, E_{13} and E_{23} separately and observing that the average values for the stresses obtained in each simulation were approximately equal. The effect of the mesh size was studied by varying the number of finite elements in the FE model. Therefore the number of degree of freedom was changed from 665,700 to 5,180,850. It was observed that using from 3,000,000 to 5,180,850 degrees of freedom led

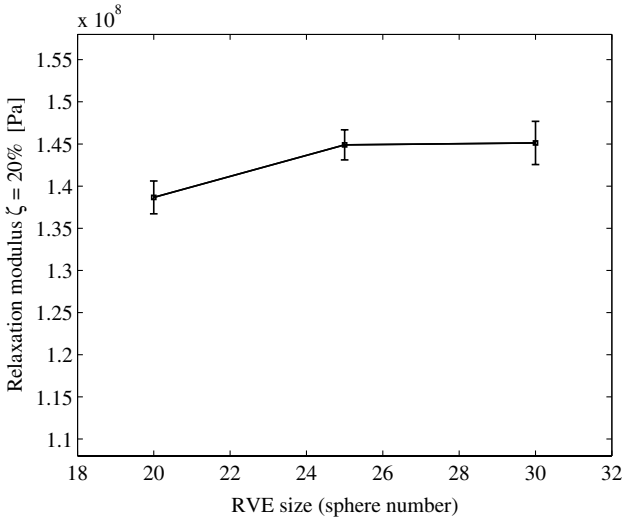

Fig. 5. Mean shear relaxation modulus for each RVE size (20, 25 and 30 spheres) at $t = 0$. $\zeta = 20\%$. The error bars are a 95% confidence interval on the mean value. $\eta = 10$.

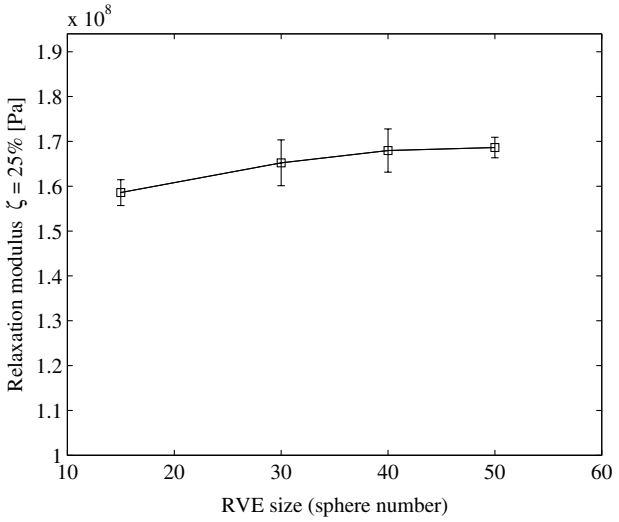

Fig. 6. Mean shear relaxation modulus for each RVE size (15, 30, 40 and 50 spheres) at $t = 0$. $\zeta = 25\%$. The error bars are a 95% confidence interval on the mean value. $\eta = 10$.

to variation in Σ_{12} of approximately 1.1%. Approximately 3,000,000 were then used for the computations. Fig. 9 shows the effect of the mesh size for $\zeta = 10\%$ with $\eta = 10$.

3. Relaxation spectra

For a linear viscoelastic and isotropic material, the shear relaxation modulus $\mu(t)$ can be expressed in a general way as (Bouleau, 1991):

$$\mu(t) = \int_0^\infty \exp\left[-\frac{t}{\tau}\right] \mathrm{d}\bar{\mu}(\tau) + \mu'' \tag{3.1}$$

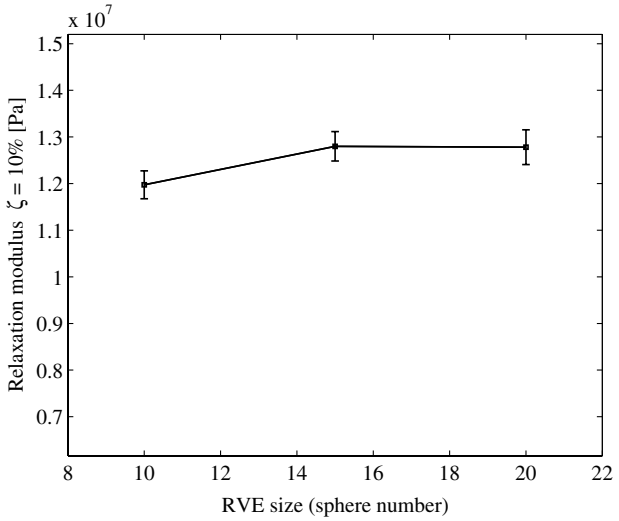

Fig. 7. Mean shear relaxation modulus for each RVE size (10, 15 and 20 spheres) at $t = 0$. $\zeta = 10\%$. The error bars are a 95% confidence interval on the mean value. $\eta = 100$.

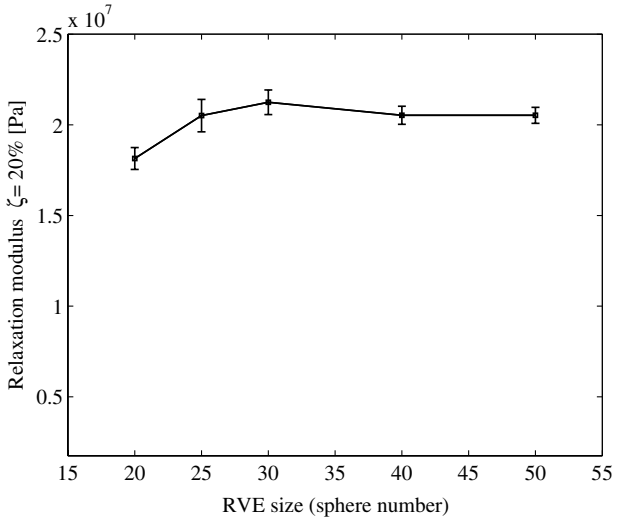

Fig. 8. Mean shear relaxation modulus for each RVE size (20, 25, 30, 40 and 50 spheres) at $t = 0$. $\zeta = 20\%$. The error bars are a 95% confidence interval on the mean value. $\eta = 100$.

where $d\bar{\mu}(\tau)$ is a positive measure in $\mathbb{R}_+^* \in]0, \infty[$ and μ'' represents the elastic response of the material ($\mu'' > 0$). These restrictions are imposed by thermodynamics. $d\bar{\mu}(\tau)$ is commonly called relaxation *spectrum*.

The relaxation spectrum may be continuous on an interval of time (even infinite) and/or constituted of Dirac impulsions. The objective of this section is to obtain the relaxation spectrum from the FE simulations. Many researchers worked on this subject considering experimental data. Some developed methods like the collocation method of Schapery (1962) which requires matrix inversions and a solution violating the principles of thermodynamics can be obtained (i.e. negative Dirac impulsions). Other methods (Emri and Tschoegl, 1993) were developed for avoiding these kind of results. However in Emri and Tschoegl (1993) an iterative process is necessary to avoid the apparition of negative Dirac impulses.

Lévesque et al. (2007) have developed a numerical algorithm for inverting the Laplace–Carson transforms encountered in the homogenization of linear viscoelastic heterogeneous materials. One of the features of the algorithm is that it leads to linear viscoelastic materials that meet the restrictions imposed by thermodynamics.

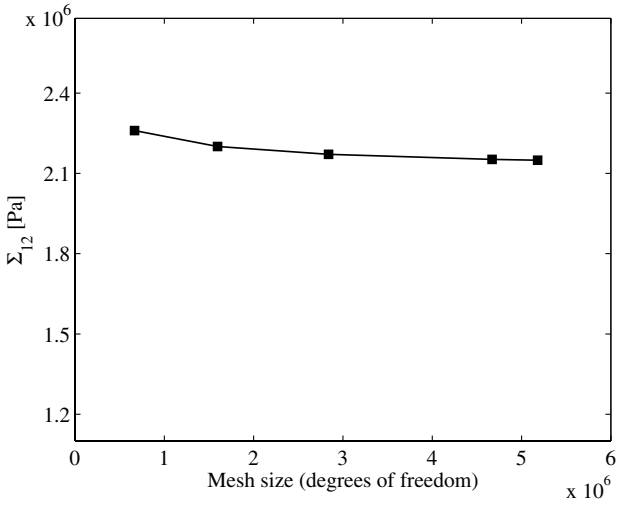

Fig. 9. Effect of the mesh size on the overall stress Σ_{12} for $\zeta = 10\%$ and $\eta = 10$.

The procedure used in this study for extracting the relaxation spectrum from the FE simulations is very similar to that algorithm. The procedure attempts finding a relaxation spectrum which is composed of Dirac impulsions and a continuous section while meeting the thermodynamics restrictions.

Relaxation spectra obtained from the analytical homogenization models are described at Section 3.1. The procedure used for obtaining the relaxation spectrum from the FE simulations is developed at Section 3.2 and tested in a case where the analytical solution is known at Section 3.3.

3.1. Relaxation spectra obtained from analytical methods

Relaxation spectra obtained from analytical homogenization techniques were generated. The homogenization models compared are: MT, SC and TOA. The viscoelastic correspondence principle was used for obtaining the overall viscoelastic effective properties. The MT model was used following the methodology of Wang and Weng (1992). For the SC model, the results of Beurthey and Zaoui (2000) and Brenner et al. (2002) were applied. Finally, for the TOA model, we applied the incompressible phases solution presented in Torquato (1998). For this model statistical parameters are needed. These parameters may be found in Torquato (1991) for a three-dimensional random distribution of totally impenetrable spheres as a function of the reinforcement volume fraction.

The MT scheme leads to a discrete spectrum constituted of two discrete lines. The relaxation spectrum obtained by the TOA model is constituted of three spectral lines. Finally, the SC scheme leads to relaxation spectrum constituted of a continuous and discrete parts. Fig. 10 shows the spectrum obtained by each method for $\zeta = 20\%$ and $\eta = 10$. It is interesting to note here that these homogenization models, for the exact same microstructure, lead to relaxation spectra of different natures. This is in fact the motivation of our study.

3.2. Relaxation spectra obtained from FE simulations

For a discrete spectrum, the shear relaxation modulus can be expressed as:

$$\mu(t) = \mu'' + \sum_{i=1}^{n_d} \mu_i \exp\left[-\frac{t}{\tau_i}\right] \tag{3.2}$$

where n_d is the number of discrete relaxation times, μ'' is the elastic response, μ_i is the spectral line intensity and τ_i is the relaxation time of the corresponding spectral line i. In our procedure, the relaxation times are defined a

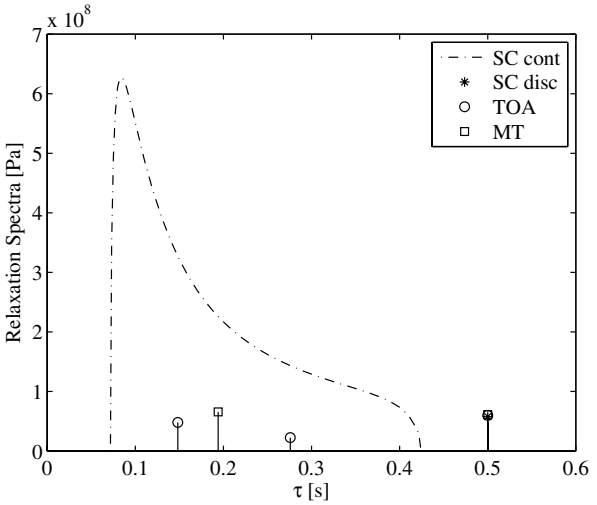

Fig. 10. Relaxation spectra obtained by applying analytical methods. $\zeta = 20\%$ and $\eta = 10$. MT: Mori-Tanaka, SC cont: Self-Consistent continuous contribution. SC disc: Self-Consistent discrete contribution. TOA: Torquato.

priori. The inverse of the relaxation times were distributed uniformly on a log scale according to Lévesque et al. (2007):

$$\frac{1}{\tau_i} = 10^{\log[(1+\theta)\theta_{\min}] + i\frac{\log[(1-\theta)\theta_{\max}] - \log[(1+\theta)\theta_{\min}]}{n_{\mathrm{d}}-1}} \quad \text{with} \quad i = 0, 1, \ldots, n_{\mathrm{d}} - 1 \tag{3.3}$$

The parameter θ defines the range over which the $\frac{1}{\tau_i}$ are distributed between $\theta_{\min}$ and $\theta_{\max}$.

In order to meet the thermodynamics restrictions, μ_i and μ'' must be positive. μ'' can be calculated by measuring the stress and the strain for a large time when the material is completely relaxed. In our case μ'' is equal to zero since both phases are Maxwellian. However, for the sake of generality, μ'' is kept in the developments since the procedure could be applied to non-Maxwellian materials. A change of variable was introduced for obtaining a positive spectrum ($\mu_i \geqslant 0$). Therefore, μ_i is defined as $\mu^2_{\mathrm{app}_i}$ and the following function has been introduced:

$$\mu^{\mathrm{d}}_{\mathrm{app}}(t) = \mu'' + \sum_{i=1}^{n_{\mathrm{d}}} \mu^2_{\mathrm{app}_i} \exp\left[-\frac{t}{\tau_i}\right] \tag{3.4}$$

The μ_{app_i} can be determined by solving the following optimization problem:

$$\inf_{\mu_{\mathrm{app}_i}} E^2_{\mathrm{d}} = \inf_{\mu_{\mathrm{app}_i}} \sum_{i=1}^{M} [\mu_{\mathrm{real}}(t_i) - \mu^{\mathrm{d}}_{\mathrm{app}}(t_i)]^2 \quad \text{with } \mu(0) = \mu'' + \sum_{i=1}^{n_{\mathrm{d}}} \mu^2_{\mathrm{app}_i} \tag{3.5}$$

where M is the number of points calculated on the relaxation curve obtained from the FE simulations, $\mu_{\mathrm{real}}(t_i)$ is the shear relaxation modulus obtained from the FE simulations and E^2_{d} is the sum of the squared differences $\mu_{\mathrm{real}}(t_i) - \mu^{\mathrm{d}}_{\mathrm{app}}(t_i)$. The constraint at Eq. (3.5) has been introduced for enforcing the real and the modeled elastic responses to be the same. This minimization problem was solved with `Mathematica` and the `Random Search` algorithm of the `NMinimize` function. This applies for all the minimization problems in this paper. In the case where a material is modeled with only a continuous spectrum, we introduced the following numerical representation:

$$H_i(\tau) = \left(\sum_{s=1}^{i-1} \Delta g(\tau_s)\right) + \left(\frac{\tau - \tau_{i-1}}{\tau_i - \tau_{i-1}} \Delta g(\tau_i)\right) \quad \text{for } \tau_{i-1} < \tau < \tau_i \tag{3.6}$$

Therefore, the shear relaxation modulus is approximated by:

$$\mu^{c}_{app}(t) = \mu'' + \sum_{i=1}^{n_c-1} \int_{\tau_i}^{\tau_{i+1}} \exp\left[-\frac{t}{\tau}\right] H_i(\tau)\,d\tau \tag{3.7}$$

The continuous spectrum is therefore a piecewise linear interpolation between the values $H(\tau_{i-1})$ and $H(\tau_i)$. Fig. 11 illustrates this function. At Eq. (3.7), n_c represents the number of $H(\tau_i)$ used in the interpolation. For imposing that $H(\tau) \geqslant 0$ the following constraints were imposed:

$$CE_i = \sum_{s=1}^{i} \Delta g(\tau_s) \geqslant 0 \quad \text{for } i = 1 \text{ to } n_c \tag{3.8}$$

The relaxation spectrum was obtained by solving this optimization problem:

$$\inf_{\Delta g(\tau_s)} E_c^2 = \inf_{\Delta g(\tau_s)} \sum_{i=1}^{m} [\mu_{real}(t_i) - \mu^{c}_{app}(t_i)]^2 \tag{3.9}$$

where E_c^2 is the sum of the squared differences $\mu_{real}(t_i) - \mu^{c}_{app}(t_i)$.

Then, an approximate function composed of a discrete and a continuous spectra can be given by:

$$\mu^{c+d}_{app}(t) = \mu'' + \sum_{i=1}^{n_d} \mu^2{}_{app_i} \exp\left[-\frac{t}{\tau_i}\right] + \sum_{j=1}^{n_c-1} \int_{\tau_j}^{\tau_{j+1}} \exp\left[-\frac{t}{\tau}\right] H_j(\tau)\,d\tau \tag{3.10}$$

The spectrum is obtained by solving the following optimization problem:

$$\inf_{\mu_{app_i}, \Delta g(\tau_s)} E^2_{c+d} = \inf_{\mu_{app_i}, \Delta g(\tau_s)} \sum_{i=1}^{m} [\mu_{real}(t_i) - \mu^{c+d}_{app}(t_i)]^2 \quad \text{with } CE_i = \sum_{s=1}^{i} \Delta g(\tau_s) \geqslant 0 \tag{3.11}$$

where E^2_{c+d} is the sum of the squared differences $\mu_{real}(t_i) - \mu^{c+d}_{app}(t_i)$.

It should be noted that the constraint $\mu_{real}(0) = \mu_{app}(0)$ was not enforced at optimization problems (3.9) and (3.11). It was found that the optimum results obtained without this constraint led to $\mu^{real}(0) \cong \mu_{app}(0)$ and therefore, this constraint is not required. In addition, relaxing this constraint decreases significantly the computational burden for solving problems (3.9) and (3.11).

The relaxation spectrum determination from the FE simulations is obtained in several steps. At first an optimum approximate discrete spectrum is obtained by solving problem (3.5). It has been observed that the SC predictions fit relatively well the FE results. For this reason, a continuous spectrum with a discrete line is optimized according to problem (3.11). Finally, the values of the τ_i for the discrete lines and the bounds of the continuous spectrum are combined and the problem (3.11) is solved anew. In all cases, the relaxation times (i.e. τ_i) and the bounds of the continuous spectrum are varied by trials and errors for obtaining a value of E^2_{c+d} that appears to be minimum. As in most nonlinear optimization problems, this procedure does not guar-

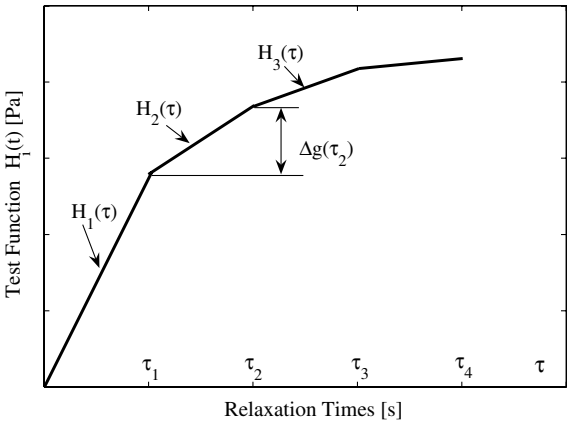

Fig. 11. Continuous test function used for approximating the relaxation spectra $\mu^{c}_{app}(t)$.

antee that an absolute minimum has been attained. It was found that it led to relaxation curves where $\mu_{app}^{c+d}(t)$ fit remarkably well the $\mu_{real}(t)$ (see Fig. 21). An example is developed in Section 3.3.

3.3. Procedure validation

For testing the procedure, the SC solution for an isotropic, incompressible and Maxwellian composite with $\zeta = 20\%$ and with the mechanical properties listed at Table 1 for $\eta = 10$ is used for generating the numerical values of the shear relaxation modulus that were used in the solution of the least square problem. In this case, the relaxation spectrum is already known and the goal is to recover it by using the procedure described above. Three steps were performed:

(i) An optimum discrete spectrum was obtained by solving problem (3.5). The parameters θ_{min} and θ_{max} at Eq. (3.3) were first optimized, by trials and errors for minimizing E_d^2. The parameter θ at Eq. (3.3) was arbitrarily set to zero. Then some relaxation times were deleted, others sligthly varied for decreasing further the value of E_d^2.
(ii) For the cases studied here it was observed that the SC solution fitted very well the FE results. Therefore, a spectrum constituted of a continuous part and a discrete line was obtained by solving problem (3.11). However, if there is not a known function that approximates well the relaxation modulus it is necessary to solve the problem (3.9). For the sake of generality, we solved problem (3.9) for testing the procedure. A continuous spectrum was obtained by finding the bounds of τ that minimizes E_c^2. The bounds of the continuous spectrum were obtained as described at the step 1 for the calculation of θ_{min} and θ_{max}. In addition, the distribution of τ_i used in the linear interpolation of the continuous spectrum was optimized.
(iii) The optimum relaxation times obtained at the step 1 and the bounds of the continuous spectrum obtained at the step 2 were combined and the procedure of trials and errors applied on the relaxation times selection for the discrete part and the range of τ for the continuous part, was repeated until the value of E_{c+d}^2 appeared to be minimum (problem 3.11).

The optimal spectrum was obtained by observing the values of E^2. A combined spectrum was obtained if $E_d^2 > E_{c+d}^2$ and $E_c^2 > E_{c+d}^2$. Even if good approximations of the relaxation modulus can be obtained regardless of the spectrum nature, the best approximation was obtained for a continuous and discrete spectra combination (μ_{app}^{c+d}). Fig. 12 shows the continuous and discrete spectra obtained: "μ_{app}^{d}" refers to the spectrum obtained

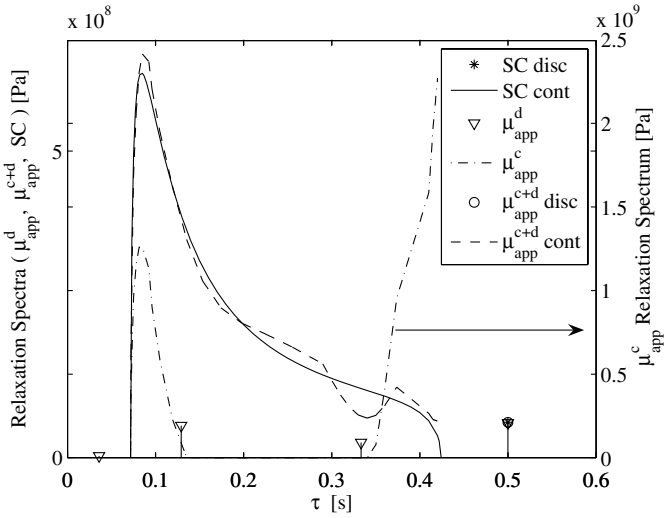

Fig. 12. Relaxation spectra obtained by the SC model and numerical approximations: μ_{app}^{d} (problem 3.5), μ_{app}^{c} (problem 3.9) and μ_{app}^{c+d} (problem 3.11). In all cases "disc" and "cont" refer to the discrete and continuous parts respectively. $\zeta = 20\%$ and $\eta = 10$. Note that the scale for μ_{app}^{c} is on the right.

by solving problem (3.5),"μ^{c}_{app}" refers to the spectrum obtained by solving problem (3.9), "μ^{c+d}_{app} disc" and "μ^{c+d}_{app} cont" refer respectively to the discrete and continuous spectra obtained by solving problem (3.11). The convergence of the continuous contribution for μ^{c+d}_{app} was difficult to obtain, even though the overall approximate spectrum shape is close the exact spectrum. This exemplifies that our procedure is capable of determining if the "real" spectrum is composed of a significant continuous part. It should be noted that the difference between the approximate and exact spectral lines intensities is approximately 0.6%. For analyzing the approximation degree of each solution the relative error between each approximation and the SC solution was calculated for each computation time. Fig. 13 shows the relative error defined as $|\frac{\mu_{real}-\mu_{app}}{\mu_{real}}|$ for each approximation. It is possible to observe that the discrete approximate solution (μ^{d}_{app}) fitted very well the values obtained by the SC method. Contrarily, the continuous approximate solution (μ^{c}_{app}) fitted the values of the SC scheme only at the first computation times. Finally, μ^{c+d}_{app} gave the best results showing that it fitted the SC values in all the time range calculated.

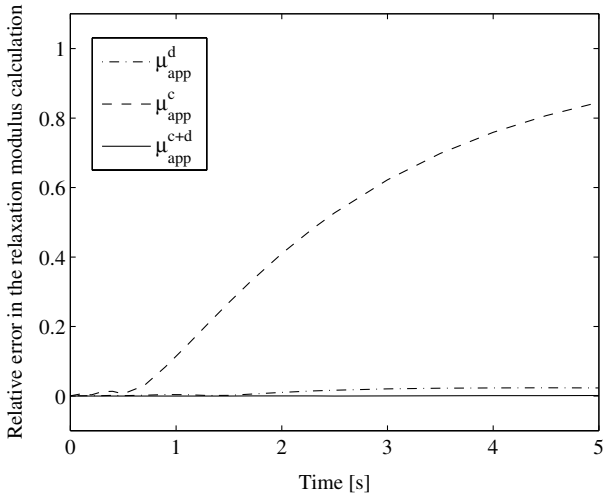

Fig. 13. Relative error in the relaxation modulus calculation with each approximate solution for each computation time. μ^{d}_{app} refers to problem (3.5), μ^{c}_{app} refers to problem (3.9) and μ^{c+d}_{app} refers to problem (3.11).

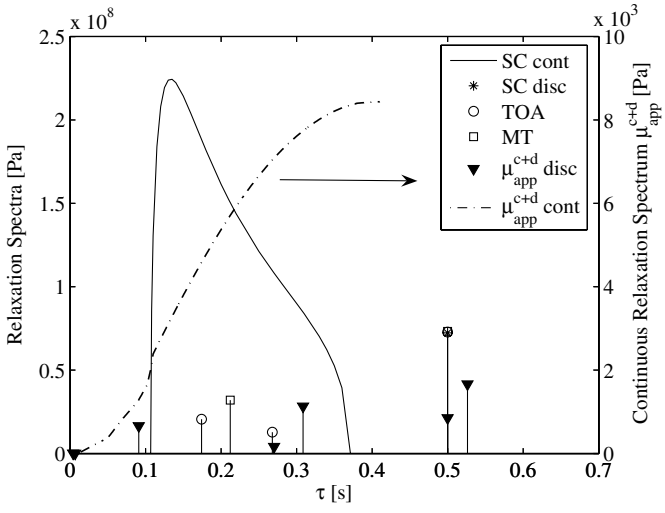

Fig. 14. Relaxation spectra obtained by different methods. $\zeta = 10\%$ and $\eta = 10$. Note that the scale for μ^{c+d}_{app}cont is on the right.

4. Results and discussions

Four volume fractions were studied with $\eta = 10$: 10%, 15%, 20% and 25% and two volume fractions with $\eta = 100$: 10% and 20%. For each volume fraction, the RVE size was established according to the procedure described at Section 2.2. The relaxation spectra of the composites simulated using the FE method were calculated with the procedure described at Section 3.2.

For the MT scheme, one of the spectral lines corresponds to the relaxation time of the soft phase (matrix) whose volume fraction is greater than the reinforcement volume fraction. Therefore, when the reinforcement volume fraction increases, the intensity on this spectral line decreases. The same behavior is observed for the SC and the TOA models. For the SC scheme the continuous part of the spectrum is of greater intensity than the spectral lines intensities and it increases with the reinforcement volume fraction.

Figs. 14–17 show the relaxation spectra obtained by different methods for linear viscoelastic composites with $\eta = 10$ for 10%, 15%, 20% and 25% volume fractions, respectively. Figs. 18 and 19 show the relaxation

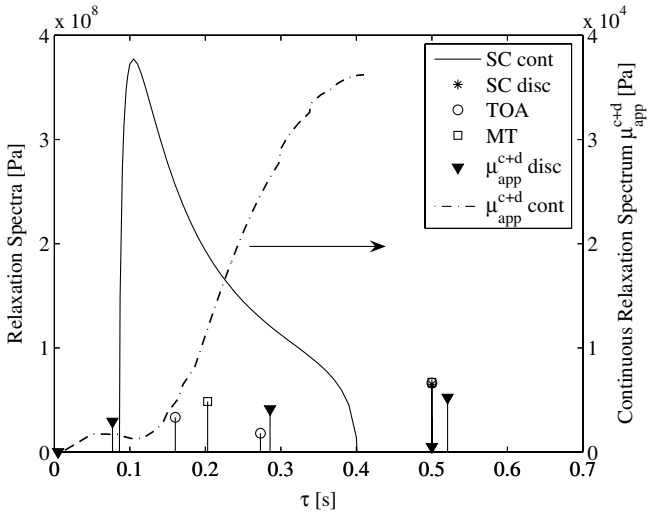

Fig. 15. Relaxation spectra obtained by different methods. $\zeta = 15\%$ and $\eta = 10$. Note that the scale for μ^{c+d}_{app}cont is on the right.

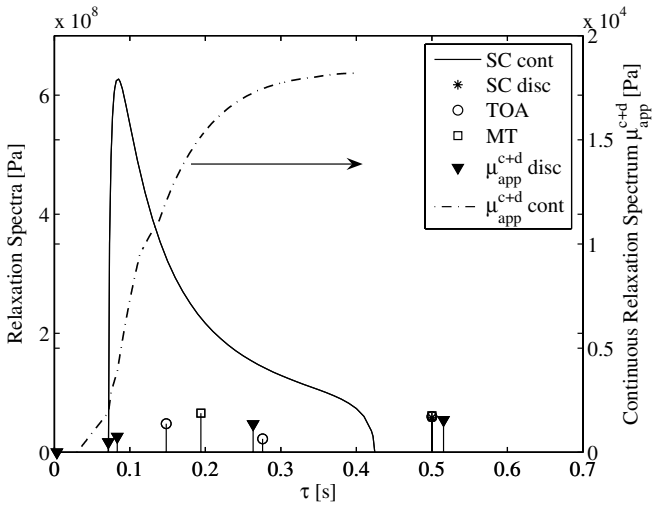

Fig. 16. Relaxation spectra obtained by different methods. $\zeta = 20\%$ and $\eta = 10$. Note that the scale for μ^{c+d}_{app}cont is on the right.

spectra obtained by different methods for linear viscoelastic composites with $\eta = 100$ for 10% and 20% volume fractions. In all cases, "SC cont" and "SC disc" refer to continuous and discrete parts of the spectra obtained with the Self-Consistent method; "TOA" refers to the spectra calculated with the Torquato technique; "MT" refers to the spectra calculated by the Mori-Tanaka model and finally "μ^{c+d}_{app} disc" and "μ^{c+d}_{app} cont" refer to discrete and continuous parts of μ^{c+d}_{app}, respectively. The right scale is related to the continuous relaxation spectrum of the numerical solution μ^{c+d}_{app}. Thus, it is possible to note the difference between the intensities of the discrete lines (left scale) and the continuous part of μ^{c+d}_{app}, which makes the continuous part negligible.

In all cases, the spectrum associated to μ^{c+d}_{app} shows one or two spectral lines close to the relaxation time associated to the matrix. The intensities of these spectral lines decrease as the volume fraction of reinforcements increases. This behavior has been observed with all the homogenization models tested in this study. The relaxation spectrum associated to μ^{c+d}_{app} is composed of a discrete spectrum and a continuous spectrum of a much lower intensity. In addition, the bounds of this continuous part are very similar to those obtained with the SC model. It would therefore seem that the relaxation spectrum "nature" of the mate-

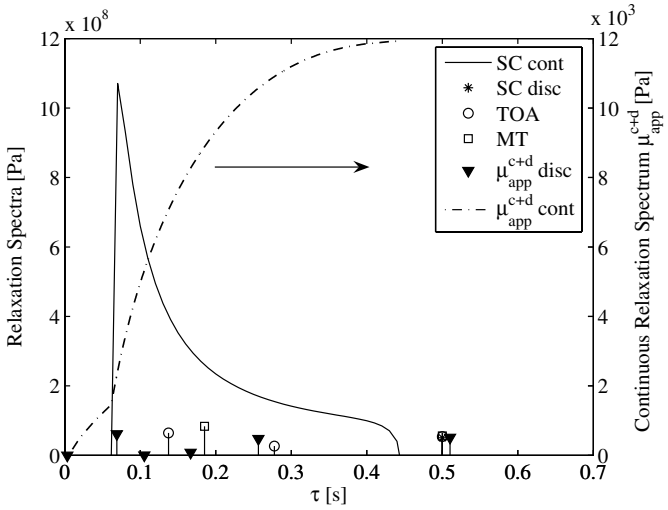

Fig. 17. Relaxation spectra obtained by different methods. $\zeta = 25\%$ and $\eta = 10$. Note that the scale for μ^{c+d}_{app}cont is on the right.

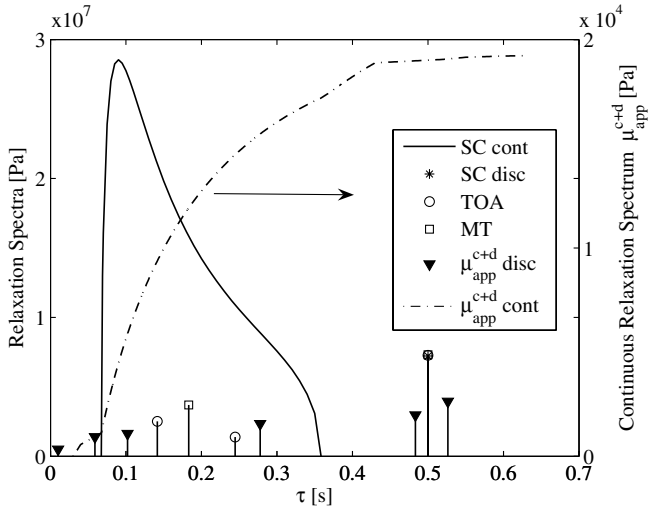

Fig. 18. Relaxation spectra obtained by different methods. $\zeta = 10\%$ and $\eta = 100$. Note that the scale for μ^{c+d}_{app}cont is on the right.

rial studied is a mixture of the homogenization models characteristics: it is composed of a dominant discrete spectrum, as in TOA and MT but also of a continuous spectrum whose bounds are very similar to the SC scheme. However, this continuous contribution is much smaller and considered as "noise" in the solution and can therefore be neglected. Fig. 20 shows the relaxation modulus obtained by using only the discrete part of μ_{app}^{c+d} and the FE results for $\zeta = 10\%$ with a $\eta = 10$ and $\eta = 100$, at the first computation times. It can be seen that the discrete part fits very well the FE results. It is also clear from these results that even if the constituent phases are Maxwellian, the resulting composite material is not, as it is predicted in analytical homogenization models.

Fig. 21 shows the relaxation curve for $\zeta = 15\%$ with $\eta = 10$ obtained for each method and the FE data for the first computation times. Only this short time interval is shown since the difference is more remarkable than at longer times. This is due to the fact that both phases are Maxwellian and that for long times the relaxation

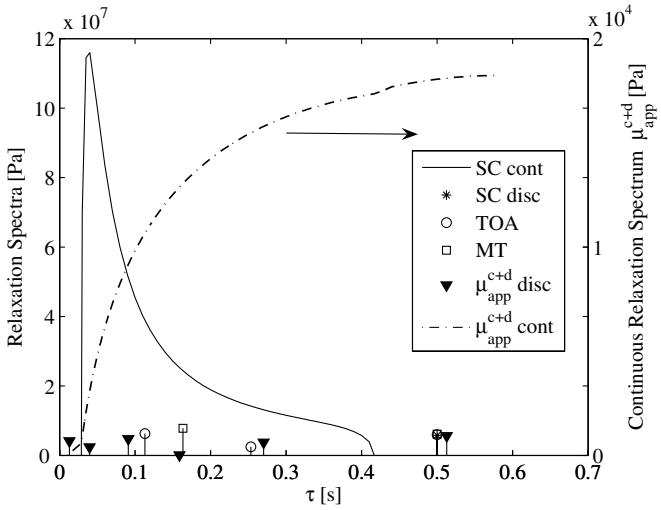

Fig. 19. Relaxation spectra obtained by different methods. $\zeta = 20\%$ and $\eta = 100$. Note that the scale for μ_{app}^{c+d}cont is on the right.

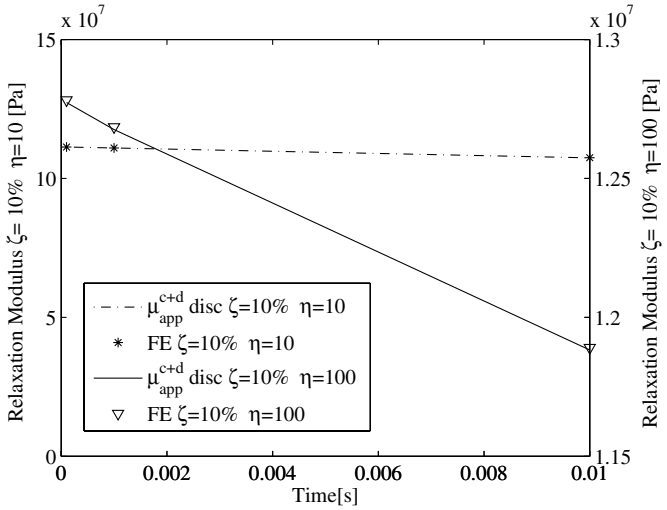

Fig. 20. Relaxation modulus calculated by the discrete part of μ_{app}^{c+d}, and the FE results for $\zeta = 10\%$ with $\eta = 10$ and $\eta = 100$.

stress in both phases is equal to zero. Similar results are obtained for the others volume fractions. It can be observed that the MT model underestimates the relaxation modulus. Amongst the analytical homogenization methods the SC method gives the best approximation to the FE data. Fig. 22 shows the relaxation modulus calculated at the first computation time for each analytical method, μ_{app}^{c+d} and the FE data for linear viscoelastic composites with $\eta = 10$. The MT model shows the maximum error in the relaxation modulus calculation, and it increases as the reinforcement volume fraction increases. The maximum error increases from 5.97% for a volume fraction $\zeta = 10\%$ to 21% for a volume fraction $\zeta = 25\%$. Fig. 23 shows the relaxation modulus calculated at the first computation time for each analytical method, μ_{app}^{c+d} and the FE results for linear viscoelastic composites with $\eta = 100$. The MT model shows again the maximum error in the relaxation modulus calculation. However, now the error introduced by all the analytical methods is greater than linear viscoelastic composites with $\eta = 10$. Therefore, the maximum error introduced by the MT model with $\eta = 100$ increases from 13.9% for $\zeta = 10\%$ to 29% for $\zeta = 20\%$.

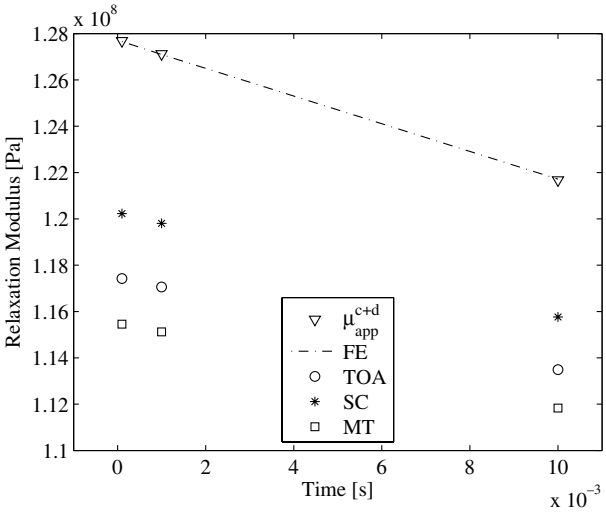

Fig. 21. Comparison of the homogenization models and the FE simulations for $\zeta = 15\%$ at first computation times. $\eta = 10$

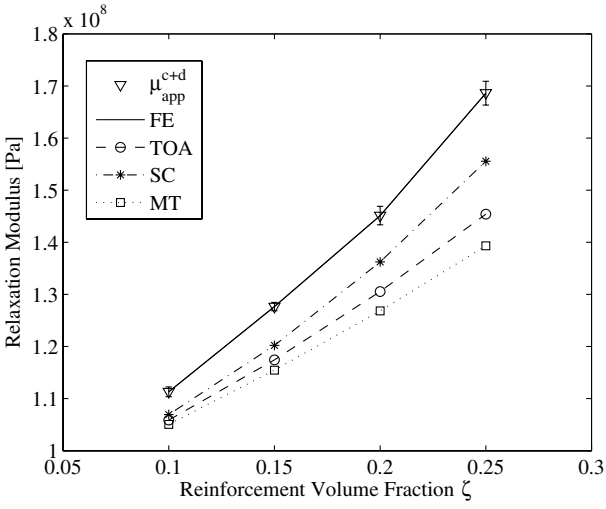

Fig. 22. Relaxation modulus calculated at the first computation time using all methods. The error bars correspond to the relative error of the FE results taking a confidence interval of 95%. $\eta = 10$.

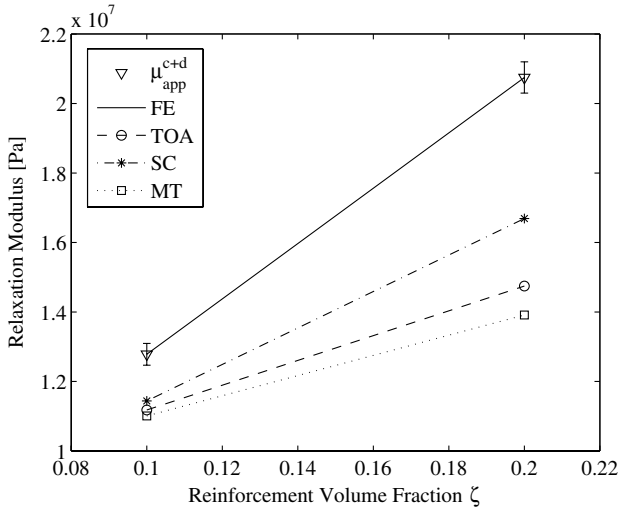

Fig. 23. Relaxation modulus calculated at the first computation time using all methods. The error bars correspond to the relative error of the FE results taking a confidence interval of 95%. $\eta = 100$.

5. Conclusions

In conclusion, the contributions of this study are:

(i) A novel procedure for the shear relaxation spectrum determination for isotropic linear viscoelastic materials that allows for a continuous as well as a discrete parts, while meeting the thermodynamics restrictions imposed on linear viscoelastic materials, to be obtained.
(ii) The comparison between FE simulations of 3D linear viscoelastic composite materials RVE and analytical homogenization models.

It is shown that the relaxation spectrum of the material studied here is composed of a dominant discrete spectrum and also from a negligible continuous spectrum. Even if the constituent phases are Maxwellian, this study confirms that, as predicted by analytical homogenization models, the effective relaxation spectrum is not of Maxwellian nature.

In this study, we only studied a composite material reinforced with randomly distributed Maxwellian reinforcements. Future work will deal with cylindrical (i.e., fibers) reinforcements as well as other viscoelastic constitutive theories in order to confirm the same trends as those observed in this study.

References

Beurthey, S., Zaoui, A., 2000. Structural morphology and relaxation spectra of viscoelastic heterogeneous media. Journal of Mechanics A/Solids 19, 1–16.

Bouleau, N., 1991. Interprétation probabiliste de la viscoélasticité linéaire. Mechanics Research Communications 19, 16–20.

Brenner, R., Masson, R., Castelneau, O., Zaoui, A., 2002. A "quasi-elastic" affine formulation for the homogenised behaviour of nonlinear viscoelastic polycrystals and composites. European Journal of Mechanics A/Solids 21, 943–960.

Brinson, L.C., Knauss, W.G., 1992. Finite element analysis of multiphase viscoelastic solids. Journal of Applied Mechanics 59 (4), 730–737.

Emri, I., Tschoegl, N.W., 1993. Generating line spectra from experimental responses. Part I: relaxation modulus and creep compliance. Rheologica Acta 32, 311–321.

Gusev, A., 1997. Representative volume element size for elastic composites: a numerical study. Journal of the Mechanics and Physics of Solids 45 (9), 1449–1459.

Hashin, Z., 1965. Viscoelastic behavior of heterogeneous media. Journal of Applied Mechanics 32 (E), 630–636.

Hazanov, S., Huet, C., 1994. Order relationships for boundary conditions effect in heterogeneous bodies smaller than the representative volume. Journal of the Mechanics and Physics of Solids 42, 1995–2011.

Huet, C., 1990. Application of variational concepts to size effects in elastic heterogeneous bodies. Journal of the Mechanics and Physics of Solids 38, 813–841.

Kanit, T., Forest, S., Galliet, I., Mounoury, V., Jeulin, D., 2003. Determination of the size of the representative volume element for random composites: statistical and numerical approach. International Journal of Solids and Structures 40, 3647–3679.

Laws, N., McLaughlin, R., 1978. Self-consistent estimates for the viscoelastic creep compliances of composite materials. Proceedings of the Royal Society of London A 359, 251–273.

Lévesque, M., Derrien, K., Mishnaevsky Jr., L., Baptiste, D., Gilchrist, M.D., 2004. A micromechanical model for nonlinear viscoelastic particle reinforced polymeric composite materials–undamaged state. Composites Part A: Applied Science and Manufacturing 35 (7), 905–913.

Lévesque, M., Gilchrist, M.D., Bouleau, N., Derrien, K., Baptiste, D., 2007. Numerical inversion of the Laplace–Carson transform applied to homogenization of randomly reinforced linear viscoelastic media. Computational Mechanics 40 (4), 771–789.

Michel, J.C., Moulinec, H., Suquet, P., 1999. Effective properties of composite materials with periodic microstructure: a computational approach. Computer Methods in Applied Mechanics and Engineering 172, 109–143.

Mishnaevsky Jr., L., 2004. Three-dimensional numerical testing of microstructures of particle reiforced composites. Acta Materialia 52 (14), 4177–4188.

Nguyen Viet, Hung, Pastor, Joseph, Muller, Didier, 1995. Method for predicting linear viscoelastic mechanical behavior of composites, a comparison with other methods and experimental validation. European Journal of Mechanics, A/Solids 14 (6), 939–960.

Schapery, R.A. 1962. Approximate methods of transform inversion for viscoelastic stress analysis. Proceedings of the 4th US National Congress on Applied Mechanics, 2, 1075–1085.

Segurado, J., LLorca, J., 2002. A numerical approximation to the elastic properties of sphere-reinforced composites. Journal of the Mechanics and Physics of Solids 50, 2107–2121.

Torquato, S., 1991. Random heterogeneous media: microstructure and improved bounds on effective properties. Applied Mechanics Reviews 44, 37–76.

Torquato, S., 1998. Effective stiffness tensor of composite media: II. Applications to isotropic dispersions. Journal of the Mechanics and Physics of Solids 46, 1411–1440.

Wang, Y.M., Weng, G.J., 1992. Influence of inclusion shape on the overall viscoelastic behavior of composites. Journal of Applied Mechanics 59, 510–518.

Xia, Z., Zhou, C., Yong, Q., Wang, X., 2006. On selection of repeated unit cell model and application of unified periodic boundary conditions in micro-mechanical analysis of composites. International Journal of Solids and Structures 43, 266–278.